Modélisation avancée des procédés de fabrication des structures composites

Brice Bognet, Chady Ghnatios, Francisco Chinesta, Adrien Leygue, Arnaud Poitou

Modélisation avancée des procédés de fabrication des structures composites

Advanced modeling of composites manufacturing processes

Brice Bognet, Chady Ghnatios, Francisco Chinesta, Adrien Leygue, Arnaud Poitou

EADS Corporate Foundation International Chair
GEM UMR CNRS – Ecole Centrale Nantes
1 rue de la Noe, BP 92101, F-44321 Nantes cedex 3, France
e-mail : Francisco.Chinestaec-nantes.fr

Résumé

Dans le cadre de la mécanique de structures nous proposons une approche 3D des modèles thermomécaniques définis dans des géométries plaque ou coque par séparation des coordonnées dans le plan et l'épaisseur, nous permettant une riche représentation 3D tout en gardant une complexité de calcul typiquement 2D.

Abstract

In the framework of structural mechanics we propose a 3D approach of thermomechanical problems defined in the degenerated geometries that constitute plates, shells or profiles. The introduction of an in-plane-out-of-plane separated representation of the unknown fields allows computing 3D solutions by keeping the 2D computational complexity characteristic of classical plate or shell theories.

Mots Clés : Représentations séparées, PGD, Réduction de modèles, Théorie de plates
Keywords: Separated representation, PGD, Model reduction, Plate theory

1. Introduction

Many models in polymer processing and composites manufacturing are defined in degenerated three-dimensional domains. By degenerated we understand that at least one of the characteristic dimensions of the domain is much lower than the other ones. This situation is particularly common in models defined in plate or shells type geometries.

When computing elastic response of plates, two dimensional plate theories are usually preferred to the numerically expensive solution of the full three-dimensional elastic problem. Going from a 3D elastic problem to a 2D plate theory model usually involves some kinematical and/or mechanical hypotheses on the evolution of the solution through the thickness of the plate.

Despite the quality of existing plate theories, their solution close to the plate edges is usually wrong as the displacement field are truly 3D in those regions and do not satisfy the kinematic hypothesis. Indeed, the kinematic hypothesis is a good approximation where Saint-Venant's principle is verified. However, some heterogeneous complex plates don't verify the Saint Venant's principle nowhere. In that case the solution of the three-dimensional model is mandatory even if its computational complexity could be out of the nowadays calculation capabilities.

Moreover, in the case of elastic behaviors the derivation of such 2D reduced models is quite simple and it constitutes the foundations of classical plate and shell theories. Today, most commercial codes for structural mechanics applications propose different type of plate and shell finite elements, even in the case of multilayered composites plates or shells. However, in composites manufacturing processes the physics encountered in such stratified plate or shell domains is much richer, because it usually involves chemical reactions, crystallization and strongly coupled and non-linear thermomechanical behaviors. The complexity of the involved physics makes impossible the introduction of pertinent hypotheses for reducing a priori the dimensionality of the model from 3D to 2D. In that case a fully 3D modeling is compulsory, and because the richness of the thickness description (many coupled physics and many plies with different physical states and directions of

anisotropy) the approximation of the fields involved in the models needs thousands of nodes distributed along the thickness direction. Thus, fully 3D descriptions may involve millions of degrees of freedom that should be solved many times because the history dependent thermomechanical behavior. Moreover, when we are considering optimization or inverse identification, many direct problems have to be solved in order to reach the minimum of a certain cost function.

Today, the solution of such fully 3D models remains intractable despite the impressive progresses reached in mechanical modeling, numerical analysis, discretization techniques and computer science during the last decade. New numerical techniques are needed for approaching such complex scenarios, able to proceed to the solution of fully 3D multiphysics models in geometrically complex parts (e.g. a whole aircraft). The well established mesh-based discretization techniques fail because the excessive number of degrees of freedom involved in the full 3D discretizations where very fine meshes are required in the thickness direction (despite its reduced dimension) and also in the in-plane directions to avoid too distorted meshes.

In this work we propose the application of the model reduction method known as Proper Generalized Decomposition - PGD- to the simulation of 3D thermomechanical models defined in plate geometries. This technique was proposed in two recent papers [1,2] for circumventing, or at least alleviating, the curse of dimensionality. This method is based on the use of separated representations. It basically consists in constructing by successive enrichment an approximation of the solution (defined in a space of dimension *d*) in the form of a finite sum of *N* functional products involving *d* functions of each coordinate. In contrast with the shape functions of classical discretization methods, these individual functions are unknown *a priori*. They are obtained by introducing the approximate separated representation into the weak formulation of the original problem and solving the resulting non-linear equations. If *M* nodes are used to discretize each coordinate, the total number of unknowns amounts to $N \times M \times d$ instead of the M^d degrees of freedom of classical mesh-based methods. Thus, the complexity of the method grows linearly with the dimension *d* of the space wherein the problem is defined, in vast contrast with the exponential growth of classical mesh-based techniques.

This strategy was successfully applied in our studies of the kinetic theory description of complex fluids. A multidimensional separated representation of the linear steady-state Fokker-Planck equation was introduced in the seminal work [1], further extended to transient simulations in [2] and non-linear Fokker-Planck equations in [3]. In [4] awe considered the solution of Fokker-Planck equations in complex flows, where space, time and conformation coordinates coexist.

The fully three-dimensional solution of models defined in degenerate domains is also an appealing field of application of the PGD. Consider the unknown field $u(x,y,z)$ defined in a plate domain Ξ. We could perform the in-plane-out-of-plane separated representation

$$u(x,y,z) \approx \sum_{i=1}^{i=N} X_i(\mathbf{x}) \cdot Z_i(z) \tag{1}$$

with $\mathbf{x} = (x,y) \in \Omega \subset \Re^2$ and $z \in I \subset \Re$. This strategy is particularly suitable when $\Xi = \Omega \times I$. More complex domains (e.g. plates with a varying thickness) can be treated by using an appropriate change of variable.

Because such decomposition involves the calculation of 2D functions $X_i(\mathbf{x})$ and 1D functions $Z_i(z)$ (these ones with a computational complexity negligible with respect to the computation of the 2D functions) we can conclude that the computational complexity of the fully 3D solution is of the same order of magnitude than the solution of 2D models.

2. In-plane-out-of-plane separated representation

In what follows we are illustrating the construction of the Proper Generalized Decomposition of a model defined in a plate domain $\Xi = \Omega \times I$ with $\Omega \subset \Re^2$ and $I = [0, H]$ considering the steady state heat transfer equation:

$$\nabla \cdot (\mathbf{K} \cdot \nabla u) = 0 \tag{2}$$

We consider that the laminate is composed of *P* different anisotropic plies each one characterized by a well-defined conductivity tensor $\mathbf{K}_i(x, y)$ that is assumed constant in the ply thickness. Moreover, and without a loss of generality, we assume the same thickness for the different laminate layers, that we denotes by *h*. Thus, we can define a characteristic function representing the position of each layer $i = 1, \cdots, P$:

$$\chi_i(z) = \begin{cases} 1 & z_i \le z \le z_{i+1} \\ 0 & otherwise \end{cases} \tag{3}$$

where $z_i = (i-1) \cdot h$. Now, the laminated conductivity can be given in the following separated form:

$$\mathbf{K}(x, y, z) = \sum_{i=1}^{i=P} \mathbf{K}_i(\mathbf{x}) \cdot \chi_i(z) \tag{4}$$

where $\mathbf{x} = (x, y) \in \Omega$. The weak form of Eq. (2) writes:

$$\int_{\Xi} \nabla u^* \cdot (\mathbf{K} \cdot \nabla u) d\Xi = 0 \tag{5}$$

with the test function u^* in an appropriate functional space. The solution $u(x, y, z) \equiv u(\mathbf{x}, z)$ is searched in the separated form:

$$u(\mathbf{x}, z) \approx \sum_{i=1}^{i=N} X_i(\mathbf{x}) \cdot Z_i(z) \tag{6}$$

In what follows we are illustrating the construction of one such decomposition. For this purpose we assume that at iteration $n < N$ the solution $u^n(\mathbf{x}, z)$ is already known:

$$u^n(\mathbf{x}, z) = \sum_{i=1}^{i=n} X_i(\mathbf{x}) \cdot Z_i(z) \tag{7}$$

and that at the present iteration we look for the solution enrichment $R(\mathbf{x}) \cdot S(z)$:

$$u^{n+1}(\mathbf{x}, z) = u^n(\mathbf{x}, z) + R(\mathbf{x}) \cdot S(z) \tag{8}$$

The test function involved in the weak form is as follows:

$$u^*(\mathbf{x}, z) = R^*(\mathbf{x}) \cdot S(z) + R(\mathbf{x}) \cdot S^*(z) \tag{9}$$

By introducing Eqs. (8) and (9) into (5) it results:

$$\int_{\Xi}\left(\begin{pmatrix}\widetilde{\nabla}R^{*}\cdot S\\ R^{*}\cdot\dfrac{dS}{dz}\end{pmatrix}+\begin{pmatrix}\widetilde{\nabla}R\cdot S^{*}\\ R\cdot\dfrac{dS^{*}}{dz}\end{pmatrix}\right)\cdot\left(\mathbf{K}\cdot\begin{pmatrix}\widetilde{\nabla}R\cdot S\\ R\cdot\dfrac{dS}{dz}\end{pmatrix}\right)d\Xi=-\int_{\Xi}\left(\begin{pmatrix}\widetilde{\nabla}R^{*}\cdot S\\ R^{*}\cdot\dfrac{dS}{dz}\end{pmatrix}+\begin{pmatrix}\widetilde{\nabla}R\cdot S^{*}\\ R\cdot\dfrac{dS^{*}}{dz}\end{pmatrix}\right)\cdot\mathbf{Q}^{n}\;d\Xi \quad (10)$$

where $\widetilde{\nabla}$ denotes the plane component of the gradient operator $\widetilde{\nabla}^{T}\equiv\left(\partial/\partial x,\partial/\partial y\right)$ and $\mathbf{Q}^{n}$ denotes the flux at iteration *n*:

$$\mathbf{Q}^{n}=\mathbf{K}\cdot\sum_{i=1}^{i=n}\begin{pmatrix}\widetilde{\nabla}X_{i}\left(\mathbf{x}\right)\cdot Z_{i}\left(z\right)\\ X_{i}\left(\mathbf{x}\right)\cdot\dfrac{dZ_{i}\left(z\right)}{dz}\end{pmatrix} \quad (11)$$

Now, as the enrichment process is non-linear we propose to search the couple of functions $R\left(\mathbf{x}\right)$ and $S\left(z\right)$ by applying an alternating direction fixed point algorithm. Thus, assuming $R\left(\mathbf{x}\right)$ known, we compute $S\left(z\right)$, and then we update $R\left(\mathbf{x}\right)$. The process continues until reaching convergence. The converged solutions allow defining the next term in the finite sums decomposition: $R\left(\mathbf{x}\right)\rightarrow X_{n+1}\left(\mathbf{x}\right)$ and $S\left(z\right)\rightarrow Z_{n+1}\left(z\right)$.

We are illustrating each one of the just referred steps:

I. Computing $R\left(\mathbf{x}\right)$ *from* $S\left(z\right)$*:*

When $S\left(z\right)$ is known the test function reduces to:

$$u^{*}\left(\mathbf{x},z\right)=R^{*}(\mathbf{x})\cdot S(z) \quad (12)$$

and the weak form (10) reduces to:

$$\int_{\Xi}\begin{pmatrix}\widetilde{\nabla}R^{*}\cdot S\\ R^{*}\cdot\dfrac{dS}{dz}\end{pmatrix}\cdot\left(\mathbf{K}\cdot\begin{pmatrix}\widetilde{\nabla}R\cdot S\\ R\cdot\dfrac{dS}{dz}\end{pmatrix}\right)d\Xi=-\int_{\Xi}\begin{pmatrix}\widetilde{\nabla}R^{*}\cdot S\\ R^{*}\cdot\dfrac{dS}{dz}\end{pmatrix}\cdot\mathbf{Q}^{n}\;d\Xi \quad (13)$$

Now, as all the functions involving the coordinate *z* are known, they could be integrated in $I=\left[0,H\right]$. Thus, if we consider:

$$\mathbf{K}=\begin{pmatrix}\mathbb{k} & \mathbf{k}\\ \mathbf{k}^{T} & \kappa\end{pmatrix} \quad (14)$$

with $\mathbb{k}=\begin{pmatrix}k_{xx} & k_{xy}\\ k_{yx} & k_{yy}\end{pmatrix}$, $\mathbf{k}=\begin{pmatrix}k_{xz}\\ k_{yz}\end{pmatrix}$ and $\kappa=k_{zz}$, then we can define:

$${}^{x}\mathbf{K}=\begin{pmatrix}\displaystyle\int_{z=0}^{z=H}\mathbb{k}S^{2}dz & \displaystyle\int_{z=0}^{z=H}\mathbf{k}\frac{dS}{dz}Sdz\\ \displaystyle\int_{z=0}^{z=H}\mathbf{k}^{T}\frac{dS}{dz}Sdz & \displaystyle\int_{z=0}^{z=H}\kappa\left(\frac{dS}{dz}\right)^{2}dz\end{pmatrix} \quad (15)$$

and

$$ {}^{x}\mathbf{Q}^{n} = \sum_{i=1}^{i=N} \begin{pmatrix} \int_{z=0}^{z=H} \mathbb{k} S Z_i dz & \int_{z=0}^{z=H} \mathbf{k} S \frac{dZ_i}{dz} dz \\ \int_{z=0}^{z=H} \mathbf{k}^T \frac{dS}{dz} Z_i dz & \int_{z=0}^{z=H} \kappa \frac{dS}{dz} \frac{dZ_i}{dz} dz \end{pmatrix} \begin{pmatrix} \widetilde{\nabla} X_i(\mathbf{x}) \\ X_i(\mathbf{x}) \end{pmatrix} \tag{16} $$

that allows writing equation (13) into the form

$$ \int_{\Omega} \begin{pmatrix} \widetilde{\nabla} R^* \\ R^* \end{pmatrix} \cdot \left({}^{x}\mathbf{K} \cdot \begin{pmatrix} \widetilde{\nabla} R \\ R \end{pmatrix} \right) d\Omega = -\int_{\Omega} \begin{pmatrix} \widetilde{\nabla} R^* \\ R^* \end{pmatrix} \cdot {}^{x}\mathbf{Q}^{n} \; d\Omega \tag{17} $$

that defines an elliptic 2D problem defined in Ω.

II. Computing $S(z)$ from $R(\mathbf{x})$:

When $R(\mathbf{x})$ is known the test function writes:

$$ u^*(\mathbf{x}, z) = R(\mathbf{x}) \cdot S^*(z) \tag{18} $$

and the weak form (10) reduces to:

$$ \int_{\Xi} \begin{pmatrix} \widetilde{\nabla} R \cdot S^* \\ R \cdot \frac{dS^*}{dz} \end{pmatrix} \cdot \left(\mathbf{K} \cdot \begin{pmatrix} \widetilde{\nabla} R \cdot S \\ R \cdot \frac{dS}{dz} \end{pmatrix} \right) d\Xi = -\int_{\Xi} \begin{pmatrix} \widetilde{\nabla} R \cdot S^* \\ R \cdot \frac{dS^*}{dz} \end{pmatrix} \cdot \mathbf{Q}^{n} \; d\Xi \tag{19} $$

Now, as all the functions involving the in-plane coordinates $\mathbf{x} = (x, y)$ are known, they could be integrated in Ω. Thus, using the previous notation, we can define:

$$ {}^{z}\mathbf{K} = \begin{pmatrix} \int_{\Omega} \left(\widetilde{\nabla} R \right) \cdot \left(\mathbb{k} \cdot \left(\widetilde{\nabla} R \right) \right) d\Omega & \int_{\Omega} \left(\widetilde{\nabla} R \right) \cdot \mathbf{k} R d\Omega \\ \int_{\Omega} \mathbf{k} \cdot \left(\widetilde{\nabla} R \right) R d\Omega & \int_{\Omega} \kappa \left(R \right)^2 d\Omega \end{pmatrix} \tag{20} $$

and

$$ {}^{z}\mathbf{Q}^{n} = \sum_{i=1}^{i=N} \begin{pmatrix} \int_{\Omega} \widetilde{\nabla} R \cdot \left(\mathbb{k} \cdot \widetilde{\nabla} X_i \right) d\Omega & \int_{\Omega} \widetilde{\nabla} R \cdot \mathbf{k} X_i d\Omega \\ \int_{\Omega} R \mathbf{k} \cdot \widetilde{\nabla} X_i d\Omega & \int_{\Omega} \kappa R X_i d\Omega \end{pmatrix} \begin{pmatrix} Z_i \\ \frac{dZ_i}{dz} \end{pmatrix} \tag{21} $$

that allows writing equation (19) into the form

$$\int_I \begin{pmatrix} S^* \\ \dfrac{dS^*}{dz} \end{pmatrix} \cdot \left({}^z\mathbf{K} \cdot \begin{pmatrix} S \\ \dfrac{dS}{dz} \end{pmatrix} \right) dz = -\int_I \begin{pmatrix} S^* \\ \dfrac{dS^*}{dz} \end{pmatrix} \cdot {}^z\mathbf{Q}^n \; dz \tag{22}$$

that defines a one-dimensional BVP defined in I .

3. Solving elastic problems

When we consider the elastic behavior of a plate, it suffices considering a separated representation of each component of the displacement vector:

$$\mathbf{u}(x,y,z) = \begin{pmatrix} u(x,y,z) \\ v(x,y,z) \\ w(x,y,z) \end{pmatrix} \approx \sum_{i=1}^{i=N} \begin{pmatrix} u_{xy}^i(x,y) \cdot u_z^i(z) \\ v_{xy}^i(x,y) \cdot v_z^i(z) \\ w_{xy}^i(x,y) \cdot w_z^i(z) \end{pmatrix} \tag{23}$$

and proceed as just described.

We are trying to compare the complexity of PGD-based solvers with respect to the standard finite element method. For the sake of simplicity we will consider a hexahedral domain discretized using a regular structured grid with respectively N_x, N_y and N_z nodes in the x, y and z directions respectively. Even if the domain thickness is much lower than the other characteristic in-plane dimensions, the physics in the thickness direction could be quite rich, mainly when we consider composites plates composed of hundreds of plies in which the complex physics involved requires fully 3D descriptions. In that case thousands of nodes in the thickness direction could be required to represent accurately the solution behavior in that direction. In usual mesh-based discretization strategies this fact induces a challenging issue because the number of nodes involved in the model scales with $N_x \times N_y \times N_z$, however, if one applies a PGD based discretization, and the separated representation of the solution involves N modes (terms in the finite sum decomposition), one should solve N 2D problems related to the functions involving the in-plane coordinates and N 1D problems related to the functions involving the thickness coordinate. The computing time related to the solution of the one-dimensional problems can be neglected with respect to the one required for solving the two-dimensional ones. Thus, the PGD complexity scales as $N \times N_x \times N_y$.

By comparing both complexities we can notice that as soon as $N_z \gg N$ the use of PGD-based discretization leads to impressive computing time savings, making possible the solution of models never until now solved, even using low performance computing platforms.

4. Numerical tests

In this section we consider the separated representation based discretization technique – PGD - widely described in the previous sections for solving a variety of test cases in order to validate its accuracy and demonstrate its ability to efficiently handle complex scenarios that would be difficult to solve using classical finite element based 3D discretizations. As explained in the previous sections, the PGD method requires the solution of several two-dimensional and one-dimensional elliptic BVP. For all the numerical results presented below these problems have been solved using a standard Galerkin method.

To validate the proposed technique we consider a square homogeneous plate depicted in Fig. 1 and we compare the classical 3D linear elastic finite element solution and the one obtained by using the

PGD with an equivalent discretization, that is, the 2D functions involving the in-plane coordinates in the PGD are approximated using the same mesh that the finite element considered on the plate surface, and the 1D functions involving the thickness coordinate when using the PGD were approximated by using the same number of nodes that was considered in the thickness finite element approximation.

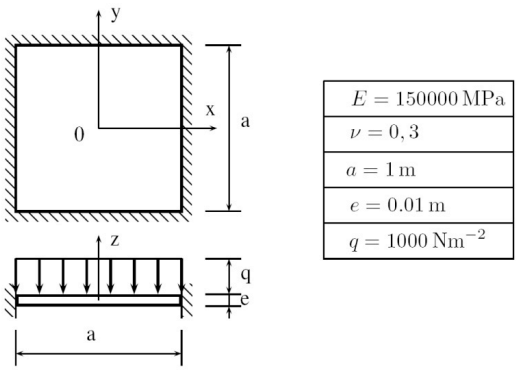

$E = 150000\,\mathrm{MPa}$
$\nu = 0,3$
$a = 1\,\mathrm{m}$
$e = 0.01\,\mathrm{m}$
$q = 1000\,\mathrm{Nm}^{-2}$

Fig. 1. Problem geometry

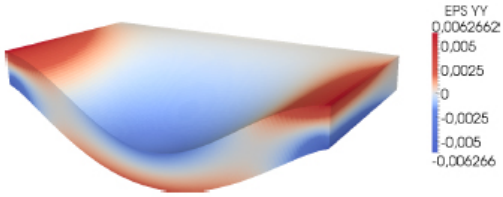

Fig. 2. Computed solution by applying the PGD - only the solution in a half of the domain is depicted for the sake of clarity -

The applied load consists of a uniform pressure applied on the upper face. The finite element solution was performed by considering a uniform mesh composed of 100×100×50 8-nodes hexahedral elements. The PGD solution was performed by using the uniform mesh composed of 100×100 4-nodes elements for approximating the functions involving the in-plane coordinates, whereas a uniform one dimensional mesh composed of 50 2-nodes 1D linear elements were used for approximating the functions involving the thickness coordinate.

The solution computed by using the PGD is depicted in Fig. 2. Nine modes were needed for approximating the solution when using the PGD, most of them to describe the 3D effects that appear in the neighborhood of the boundaries where the displacement was prescribed. In order to compute these 9 terms involved in the separated representation 165 2D and 1D problems were solved. Fig. 3 shows the energy density error, considering as reference solution the one computed by using the FEM. This error is everywhere lower than 0.3% except in the vicinity of the plate corners where it reaches a value of 0.57 %. This error can be reduced by considering more terms in the separated representation, i.e. higher N in the finite sum decomposition.

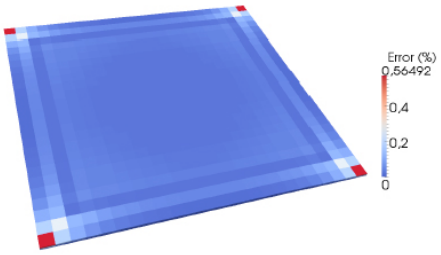

Fig. 3. Error with respect to the FEM solution considering the usual energy norm.

Because the alternative solution of 2D and 1D problems involved in the PGD solver, one could consider very different resolutions in both approximations, that is, the characteristic size of the mesh used for solving the 2D problems does not affect to the characteristic mesh considered in the approximation of functions involving the thickness coordinate, and viceversa. Moreover, one could use different discretization techniques for solving both problems.

Figure 4 compares the CPU time of both the PGD and the FEM based discretizations for solving the linear elasticity problem previously described as a function of the number of in-plane degrees of freedom, $N_x \times N_y$ and of the number of degrees of freedom in the thickness, N_z. We can notice the linear evolution of the computational complexity with the number of in-plane or out-of-plane degrees of freedom when using the PGD instead the exponential growing when using the finite element discretization.

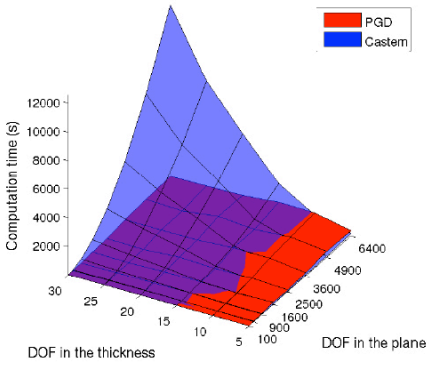

Fig. 4. Comparison of the PGD and FEM based 3D discretizations.

In this simple problem, the edge effects are already present and confirm the necessity of several modes to correctly describe the solution in the boundary neighborhood. In Fig. 5 and Fig. 6 we depict respectively the first and the second mode of the PGD solution. The first mode seems to represent classical plate theory solutions because the first mode of the displacements $u_z^1(z)$, $v_z^1(z)$ and $w_z^1(z)$ shows a linear evolution in the thickness direction.

The second mode of the PGD solution shows a more complex z-dependence but it should be noticed that in the xy-plane it essentially contributes to the solution in the plate edges neighborhood where one expect to observe a truly 3D displacement field. The subsequent modes of the PGD solution gradually improve the solution quality close to the plate edges and corners.

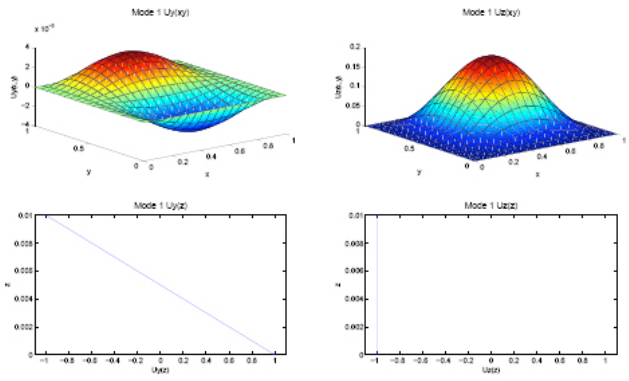

Fig. 5. First mode of the PGD solution. Left: $v_{xy}^1(x,y)$-top- and $v_z^1(z)$-down-. Right: $w_{xy}^1(x,y)$-top- and $w_z^1(z)$-down-.

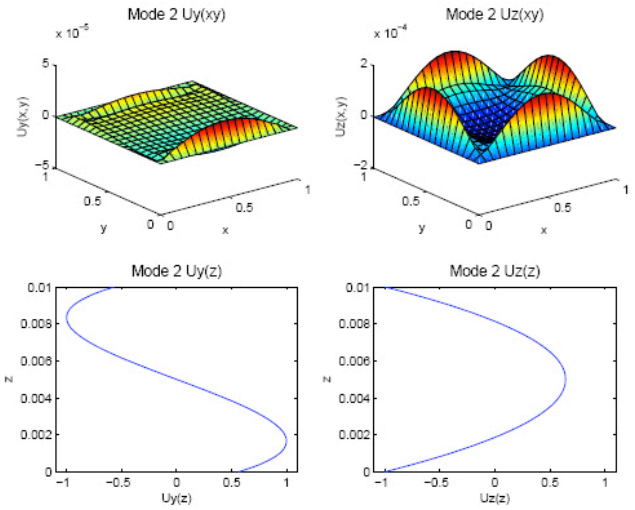

Fig. 6. Second mode of the PGD solution. Left: $v_{xy}^2(x,y)$*-top- and* $v_z^2(z)$*-down-. Right:* $w_{xy}^2(x,y)$*-top- and* $w_z^2(z)$*-down-.*

The same procedure can be applied for solving more complex structures as multilayered composites and honeycomb composites structures as depicted in Figs. 7, 8 and 9.

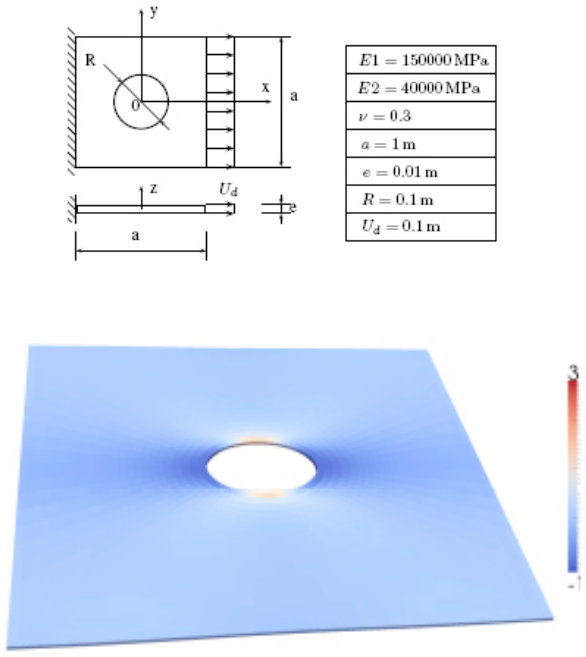

Fig. 7. PGD solution of a multilayered composite plate composed of 16 unidirectional plies.

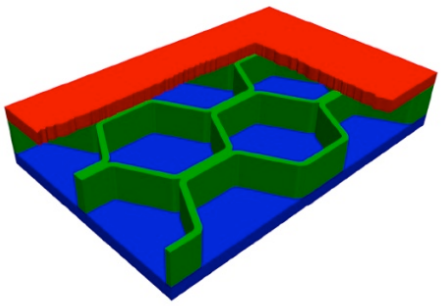

Fig. 8. Honeycomb composite structure.

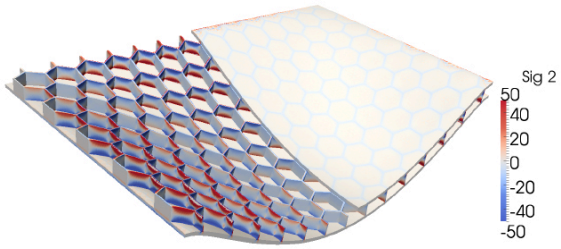

Fig. 9. PGD solution of a honeycomb composite structure.

Références

[1] A. Ammar, B. Mokdad, F. Chinesta, R. Keunings, "A new family of solvers for some classes of multidimensional partial differential equations encountered in kinetic theory modeling of complex fluids," J. Non-Newtonian Fluid Mech., vol 139, pp. 153-176, 2006.

[2] A. Ammar, B. Mokdad, F. Chinesta, R. Keunings, "A new family of solvers for some classes of multidimensional partial differential equations encountered in kinetic theory modeling of complex fluids. Part II: transient simulation using space-time separated representations," J. Non-Newtonian Fluid Mech., vol. 144, pp. 98-121, 2007.

[3] B. Mokdad, E. Pruliere, A. Ammar, F. Chinesta,"On the simulation of kinetic theory models of complex fluids using the Fokker-Planck approach," Applied Rheology, vol. 17, n. 2, pp. 26494: 1-14, 2007.

[4] B. Mokdad, A. Ammar, M. Normandin, F. Chinesta, J.R. Clermont, "A fully deterministic micro-macro simulation of complex flows involving